

# Personal Authentication Technique with Human Iris Recognition using Wavelet Transform and Coding

Wen-Shiung Chen

Department of Electrical Engineering, National Chi Nan University, Nantou 545 Taiwan

Kun-Huei Chih

Department of Electrical Engineering, National Chi Nan University, Nantou 545 Taiwan

**Abstract** – This paper presents a biometric recognition system based on the iris of a human eye using wavelet transform. The proposed system includes three modules: image preprocessing, feature extraction, and recognition modules. Image preprocessing module uses some image processing algorithms to localize the region of interest of iris from the input image. The feature extraction module adopts the gradient direction (i.e., angle) of wavelet transform vector as the discriminating texture features. The system encodes the features to generate its iris feature codes by using two efficient coding techniques: binary Gray encoding and delta modulation. Finally, the system applies these feature codes for iris matching in recognition module. The experimental results show that the system has an encouraging performance on the CASIA database (including 756 images from 108 classes). The recognition rates up to 95.27%, 95.62%, and 96.21%, respectively, by using different coding methods are achieved. Even under the circumstance of false acceptance rate (FAR) 0%, the system still approaches the recognition rates above 90% (acceptance of authentic, AA). This paper analyzes the results of the experiments to verify the related inferences of the proposed system and provides useful information for further work.

**INDEX TERMS** – BIOMETRICS, IRIS RECOGNITION, IDENTIFICATION, PERSONAL VERIFICATION, PERSONAL AUTHENTICATION, WAVELET TRANSFORM, MULTI-SCALE ANALYSIS, DELTA MODULATION.

## 1. INTRODUCTION

Personal authentication (or identity authentication) is critical in a wide range of applications such as i) military, ii) forensics: criminal identification and personal security, and iii) civilian: national ID card, passport, computer login systems, home security systems, ATMs, credit cards, and so forth [1]. The traditional methods for personal authentication are based on what a person possesses (key, ID card, etc.) or what a person knows (secret password, PIN number, etc.).

However, there are some problems in these methods. For example, keys may be falsified, ID cards may be lost, passwords may be forgotten, and so on. Accurate and reliable personal authentication technique is becoming more and more urgent to the operation of cybernetic society [1] [2]. How does the machine know the person who holds the password is the person he claims to be? The best way to identify a person is that

the person shows his own biometric characteristics. Recent advances in computer hardware and software technology have enabled academy and industry to develop affordable automatic biometric-based authentication systems.

Biometrics [1] refers to automatic identity authentication of a person on a basis of one's unique physiological or behavioral characteristics and is inherently more suitable for discriminating between an authorized person and an impostor than traditional methods. Under such circumstances, biometrics offers the most secure means to automatically identify individuals without requiring them to carry ID cards or memorize passwords.

In principle as well as in practice, any human physiological or behavioral trait that satisfies the high universality, high uniqueness, high permanence, high collectability, high performance, high acceptability, and high circumvention, can be employed to develop a personal identification. To date, many biometric features, including fingerprints [3], hand geometry or palmprint [4], face [5], handwritten signature [6], voice [7], DNA [8], retina [9], and iris [10]-[21], have been studied and applied to the authentication of individuals.

However, a major concern in the development of biometric-based authentication techniques is how to avoid rejecting valid users (authentics) or approving imposters (fakers). Basically, a biometric-based authentication system is essentially a pattern recognition system that determines the authenticity of a specific physiological or behavioral trait possessed by the user. Typically, automatic biometric-based authentication systems are classified into two major categories: one-to-one (or verification) and one-to-many (or identification) [1].

Most of the existing techniques have limited capabilities in recognizing relatively complex features in realistic situations. In recent years, the human iris has been receiving growing interest due to its high uniqueness, high permanence, and high circumvention.

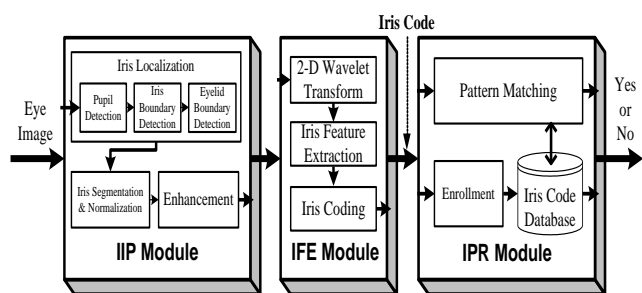


Figure 1. Structure diagram of the proposed iris recognition system.

The iris, a kind of physiological biometric feature with genetic independence, contains extremely information-rich physical structure and unique texture pattern, and thus is highly complex enough to be used as a biometric signature [14]. Intrinsically, human iris is an enormous complex meshwork of pectinate ligament tissue resulting in patterns of almost infinite variety. Statistical analysis of faker and authentic scores reveals that irises have an exceptionally high degree-of-freedom up to 266 (much more than fingerprint, showing about 78) [1], and thus are the most mathematically unique feature of the human body; more unique than fingerprint and DNA. The highly randomized appearance of the iris makes its use as a biometric well recognized. This characteristic shows that the probability of finding two persons with identical iris patterns is almost zero.

Compared with other biometric features such as hand and fingerprint, iris patterns are more stable and reliable. Each person's irises are unique, and they are stable with age [10], [14]. In addition, several studies have shown that normal variations in coloring and structure of the tissues of an iris are so multitudinous that no two irises are ever alike - not even our own or identical twins [14]. As a result, the human iris promises to deliver a high level of uniqueness to authentication applications that other biometrics cannot match. Furthermore, iris recognition systems can be non-invasive to their end-users. In short, the iris has strong potential biometric feature for identity authentication. A human iris may provide a solution to personal authentication by offering a much more discriminating biometric feature than some other techniques such as fingerprint or face recognition. In this paper, we investigate and design an automatic biometric recognition system using the human iris.

In this paper, we present a personal identification technique with iris recognition based on wavelet transform. In the feature extraction module, we select the information of the gradient direction of wavelet transform vector as the discriminating texture features. The system encodes the features by generating binary Gray codes and delta modulation. Then applying these

feature codes for iris matching in recognition module. Following the introduction in Section I, the remainder of this paper is organized as follows. In Section 2, we review the previous research. Section 3 presents the system architecture and pre-processing module of the novel iris recognition technique. Section 4 proposes two iris feature extraction methods. The experimental results are shown in Section 5. Finally, Section 6 makes a conclusion.

## 2. PREVIOUS RESEARCH

Much research in the emerging field of biometrics has focused on identification applications. Nowadays, iris has a high potential in becoming the focus of a relatively new biometric means of authentication. Nevertheless, literature shows that less work in biometric iris focusing on authentication applications has been done. After Flom and Safir [10] observed the fact that every iris has a highly detailed and unique texture that remains stable over decades of life, they proposed the concept of automated iris recognition in 1988, however, finally not realized. Early work toward actually realizing an automated iris recognition system was carried out by Johnson in 1991 [11]. In 1993 Daugman developed a successful system by using the 2-D Gabor wavelet transform [12]. Daugman's system does not use a rotation invariant representation. Rather, he performs a brute force search across a range of accepted rotations. In this system, the visible texture of a person's iris in a real-time video image is encoded into a compact sequence of multi-scale quadrature 2-D Gabor wavelet coefficients, whose most significant bits consist of a 256-byte "iris code." Daugman claimed that his system has an excellent performance on a diverse database of many iris images. In 1996, Wildes, *et al.* developed a prototype system based on an automated iris recognition that uses a very computationally demanding image registration technique [13]. This system exploits normalized correlation over small tiles within the Laplacian pyramid bands as a goodness of match measure. According to these articles, both systems have shown their promising performances on diverse databases of hundreds of iris images. A survey article discussed and compared these two systems [14]. The article in [15] discussed a commercial iris identification system based mainly on Daugman's technique in [12]. In 2010, Chou, *et al.*, developed a non-orthogonal view iris recognition system [16].

Literature shows that four approaches have also been conducted, which all are based on multi-resolution wavelet analysis. Boles and Boashash [17] proposed an iris identification system in which zero-crossing of the wavelet transform at various resolution levels is calculated over concentric circles on the iris, and the resulting 1-D signals are compared with the model features using different dissimilarity

functions. Zhu, Tan, and Wang [18] proposed an algorithm for global iris texture feature extraction using multi-channel Gabor filtering and wavelet transform. The mean and standard deviation of each sub-image at different resolution levels are extracted as the features. Their algorithm uses only a few selected resolutions for matching, thus making it computationally efficient and less sensitive to noise. Subsequently, Ma, Wang and Tan [19] modified the work in [18] by using a bank of circular symmetric filters to extract much more local texture information. They claimed that their new method competes with Daugman's method and performs better than Wildes's method. The work in [20] also uses wavelet multi-resolution analysis based on Gabor filtering for iris feature extraction. Lim, *et al.* [21] used wavelet transform to make a feature vector compact and efficient. They proposed two straightforward mechanisms such as the weight vector initialization and the winner selection for a competitive learning VQ method. Nabti and Bouridane also proposed an effective and fast iris recognition system based on a combined multi-scale feature extraction technique [22]. In summary, all of the studies discussed previously are based upon the multi-resolution analysis technique. To design an automatic iris recognition system by using an alternative of iris feature extraction is a worthwhile research issue.

### 3. SYSTEM ARCHITECTURE AND PRE-PROCESSING

#### 3.1 System Overview

The proposed framework consists of three modules: image pre-processing, feature extraction, and recognition modules, as shown in Figure 1. Since the system is tested on the CASIA iris image database [23], this paper takes no account of the iris image acquisition module. The entire system flow is briefly described as follows. First, the iris image pre-processing module (IIP module) employs some image processing algorithms to demarcate the region of interest (i.e., iris zone) from the input image containing an eye. It performs three major tasks including iris localization, iris segmentation & normalization, and enhancement for the input iris image. Next, the feature extraction module (IFE module) performs a 2-D wavelet transform, computes the gradient direction features, and applies appropriate coding methods on these features to generate the iris feature code. Finally, the iris pattern recognition module (IPR module) employs a minimum distance classifier according to Hamming distance or Euclidean distance metric to recognize the iris pattern by comparing the iris code with the enrolled iris codes in the iris code database.

#### 3.2 Pre-processing Module

Input image does contain not only useful information from iris zone but also useless data derived from the surrounding eye region. Figure 2 shows some iris image examples of human eyes. Before extracting the features of an iris, the input image must be pre-processed to localize, segment and enhance the region of interest (i.e., iris zone). The system normalizes the iris region to overcome the problem of a change in camera-to-eye distance and pupil's size variation derived from illumination. Furthermore, the brightness is not uniformly distributed due to non-uniform illumination, the system must be capable of removing the effect and further enhancing the iris image for the following feature extraction. Hence, the pre-processing module consists of three units: iris localization, iris segmentation/normalization, and enhancement, as shown in Figure 3.

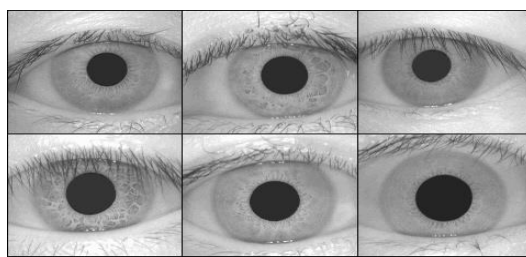


Figure 2. Some iris image examples of human eyes.

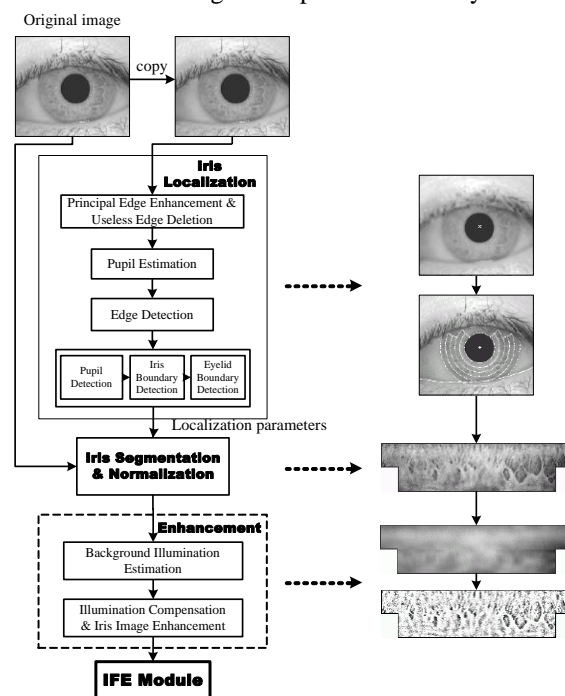


Figure 3. Pre-processing module.

### 3.2.1 Iris Localization Unit

In this unit, we must first determine the useful part (i.e., iris) from an input image. The iris is an annular region between the pupil and the sclera. The inner and outer boundaries of an iris can be treated as non-concentric circles approximately. In order to make the iris localization efficient, the system performs an operation of enhancing principal edges and blurring useless edges on the copied image instead of the original one. Following that, the system estimates the center coordinates of the pupil first. Since the pupil typically is darker than the iris and its gray level distribution has a small variance, the system uses a  $30 \times 30$  mean filter to find the location which has the minimum mean value in the image. This location is considered as an internal point of the iris region, namely the fitting point. Then the system can determine a certain region starting from the fitting point by using the iris localization procedure.

Since there exist obvious intensity differences around each boundary, a proper edge detection method is applied to find the edge points in this region, and evaluate the exact circle parameters (including the inner and outer boundaries of iris) for all possible point triplets of the edge points. According to Euclidean geometry, by calculating two perpendicular bisectors of any edge point triplet, the system can easily obtain the crossover point of two perpendicular bisectors. Select the center point as the most frequently crossed point (see Figure 4). After finding the central points of two circles, we determine the inner and outer radii of the iris by computing the distances between the central points and the inner edge points, and outer edge points, respectively. Eventually, an iris zone can be located by these parameters, as shown in Figure 5(a).

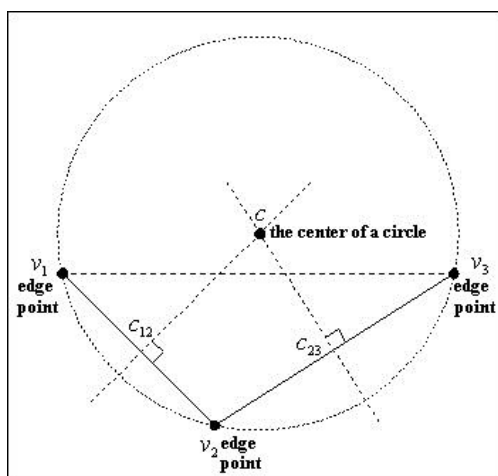
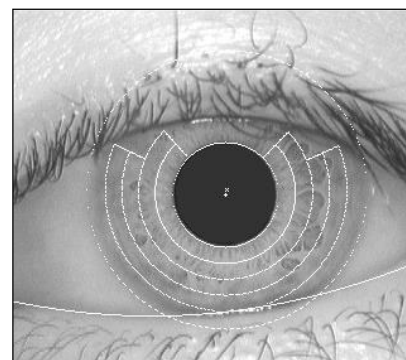
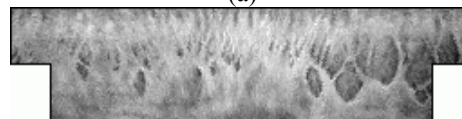


Figure 4. Illustration of finding the center of a pupil.



(a)



(b)



(c)

Figure 5. An example of image preprocessing module. (a) Localized image. (b) Segmented and normalized image. (c) After enhancement.

### 3.2.2 Iris Segmentation and Normalization Unit

The localized iris zone demarcated from the human eye is transformed from rectangular into polar coordinate system so as to facilitate the following feature extraction module. When acquiring the human eye image, the iris zone images may be in different sizes (outer and inner boundaries of iris) due to the variations of camera-to-eye distance and/or environment's illumination. The variations will change the patterns of iris texture to some extent. To solve this problem, it is necessary to compensate for the iris deformation. Daugman's system uses radial scaling to compensate for overall size as well as a simple model of pupil variation based on linear stretching [12].

This scaling serves to map Cartesian image coordinates to dimensionless polar image coordinates (see Figure 6). In addition, eyelids and eyelashes generally obscure the upper limbus of an iris, the procedure cut out the obscured area. The system generates a rectangular iris image of a fixed size by linear interpolation. The iris image is partitioned into two ring areas with equal width, the first area is with the size  $256 \times 32$  and the other area with the size  $212 \times 32$ . Figure 5(b) shows an example of the iris segmentation and normalization.

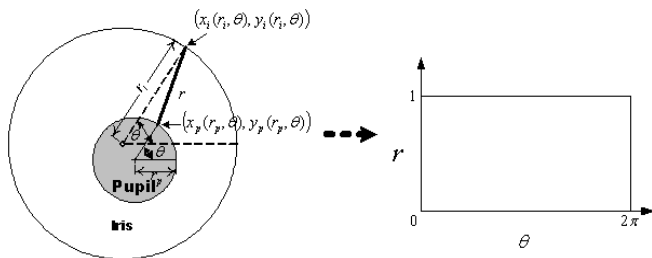


Figure 4. Mapping of Cartesian image coordinates to dimensionless polar coordinates.

### 3.2.3 Enhancement Unit

The normalized iris is easily affected by the non-uniform illumination and may have low contrast. The final step of the IIP module is to perform image enhancement in order to obtain a good-quality image which presents clearer texture. The enhancement algorithm used in this unit is to subtract the estimated background illumination from the normalized iris image to compensate for the non-uniform illumination. The background illumination is simply estimated by computing the mean of a corresponding 16x8 small block. Finally, this unit partitions the image into several 64x32 regions and enhances them with histogram equalization. Figure 5(c) shows the preprocessed human eye image which has more distinct texture characteristics.

## 4. THE PROPOSED IRIS RECOGNITION

### 4.1 Wavelet Transform-based Edge Detection

The wavelet transform has been widely used in the last few years to solve the intrinsic redundancies that appear in a multi-scale analysis [24][25][26][27]. In this paper, we have analyzed the different scale information given by the wavelet transform to acquire the abundant edge information in the iris image  $f(x, y)$ . A multi-scale version of this edge detector is designed by smoothing the surface with a convolution kernel  $\theta(x, y)$  that is dilated. This is computed with two wavelets that are the partial derivatives of  $\theta$ :

$$\psi^1(x, y) = -\frac{\partial \theta}{\partial x}, \psi^2(x, y) = -\frac{\partial \theta}{\partial y}.$$

The scale varies along the dyadic sequence  $\{2^j\}_{j \in \mathbb{Z}}$  to limit computations and storage. For the scale  $2^j$ , we denote

$$\theta_{2^j}(x, y) = 2^{-j} \theta(2^{-j}x, 2^{-j}y)$$

and

$$\overline{\theta}_{2^j}(x, y) = \theta_{2^j}(-x, -y).$$

In the two directions ( $x$ -direction and  $y$ -direction), the dyadic wavelet transform of  $f \in L^2(\mathbb{R})$  at  $(u, v)$  is

$$W_{2^j}^k f(u, v) = \langle f(x, y), \psi_{2^j}^k(x - u, y - v) \rangle \quad (1)$$

We thus derive from (1) that the wavelet transform components are proportional to the coordinates of the gradient vector of  $f$  smoothed by  $\overline{\theta}_{2^j}$ :

$$\begin{pmatrix} W_{2^j}^1 f(u, v) \\ W_{2^j}^2 f(u, v) \end{pmatrix} = 2^j \begin{pmatrix} \frac{\partial}{\partial x} (f * \overline{\theta}_{2^j})(u, v) \\ \frac{\partial}{\partial y} (f * \overline{\theta}_{2^j})(u, v) \end{pmatrix} = 2^j \vec{\nabla} (f * \overline{\theta}_{2^j})(u, v) \quad (2)$$

The modulus of this gradient vector is proportional to the wavelet transform modulus

$$M_{2^j} f(u, v) = \sqrt{|W_{2^j}^1 f(u, v)|^2 + |W_{2^j}^2 f(u, v)|^2} \quad (3)$$

Let  $A_{2^j} f(u, v)$  be the angle of the gradient direction (wavelet transform) vector (Eq. (2)) in the plane  $(x, y)$

$$A_{2^j} f(u, v) = \tan^{-1} \left( \frac{W_{2^j}^2 f(u, v)}{W_{2^j}^1 f(u, v)} \right) \quad (4)$$

The unit vector  $\vec{n}_j(u, v) = (\cos A_{2^j} f(u, v), \sin A_{2^j} f(u, v))$  is co-linear to  $\vec{\nabla} (f * \overline{\theta}_{2^j})(u, v)$ . An edge point at the scale  $2^j$  is a point  $\gamma$  such that  $M_{2^j} f(u, v)$  is local maximum at  $(u = u_\gamma, v = v_\gamma)$  when  $(u = u + \lambda \vec{n}_j(u_\gamma), v = v + \lambda \vec{n}_j(v_\gamma))$  for  $|\lambda|$  small enough. These points are also called wavelet transform modulus maxima. The criterion for detecting edge is summarized as follows:

- Step 1. Computing the  $x$ -direction WT (i.e.,  $W_{2^j}^1 f(u, v)$ ) and the  $y$ -direction WT (i.e.,  $W_{2^j}^2 f(u, v)$ ).
- Step 2. Computing the WT modulus (i.e.,  $M_{2^j} f(u, v)$ ) and the WT gradient direction (i.e.,  $A_{2^j} f(u, v)$ ).
- Step 3. Set a threshold  $T$ . The pixel point  $(x, y)$  is an edge point if (i)  $|M_{2^j} f(u, v)| \geq T$  and (ii)  $M_{2^j} f(u, v)$  is the local maximum along the direction of  $A_{2^j} f(u, v)$ .

### 4.2 Feature Extraction with Wavelet Transform

The edge structures in iris images are often the most important features for pattern recognition and clear at a variety of scales. To capture the spatial details of an image, it is advantageous to make use of a multi-scale representation. The wavelet transform is capable of focusing on localized structures with a zooming procedure that progressively reduces the scale parameter. In the paper, we extract the angle of the gradient direction (Eq. (4)) of the wavelet transform as the iris feature and encode it efficiently.

First, we apply wavelet transform on the iris image and compute the angle of the gradient direction at a specific scale.

In this paper, we use quadratic spline function (Figure 7(b)) as the wavelet function, which is the derivative of the cubic spline function shown in Figure 7(a) [25][26]. The scaling function (smoothing function) is defined as

$$\theta(x) = \begin{cases} 8(x^3 - x^2) + \frac{4}{3} & 0 \leq |x| \leq \frac{1}{2} \\ -\frac{8}{3}(x - 1)^3 & \frac{1}{2} < |x| \leq 1 \\ 0 & |x| > 1 \end{cases} \quad (5)$$

And the wavelet function is easily obtained as

$$\psi(x) = \begin{cases} 8(3x^2 - 2x) & 0 \leq |x| \leq \frac{1}{2} \\ -8(x - 1)^2 & \frac{1}{2} < |x| \leq 1 \\ 0 & |x| > 1 \end{cases} \quad (6)$$

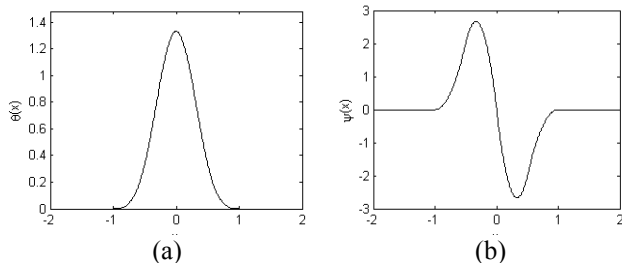


Figure 7. (a) Cubic spline function. (b) Quadratic spline wavelet function.

Edge points are distributed along curves that often correspond to the boundary of important structures. Individual wavelet modulus maxima are chained together to form a curve that follows an edge. At any location, the tangent of the edge curve is approximated by computing the tangent of the angle of the gradient direction [24]. Thus, we select the angle of the gradient direction as the iris feature for recognition. It is advantageous because the gradient direction will not be affected by contrast and illumination of the input images. Figure 8 shows the iris images of  $x$ -direction WT  $W_{2^j}^1 f(u, v)$ ,  $y$ -direction WT  $W_{2^j}^2 f(u, v)$ , WT modulus  $M_{2^j} f(u, v)$ , and WT gradient direction  $A_{2^j} f(u, v)$  obtained by quadratic spline wavelet transform for the scales  $j=1, 2, 3$ . Since singularities and irregular structures in iris images often carry essential information, we adopt two different representations, including 2-D Gray encoding and 1-D delta modulation encoding, based on the edge detection with wavelet transform in this module to extract and encode the features from a human iris image.

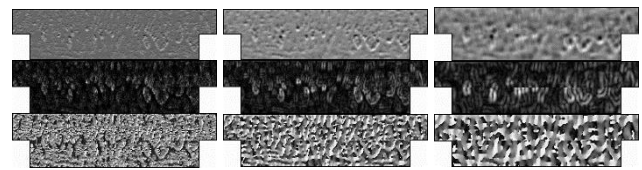
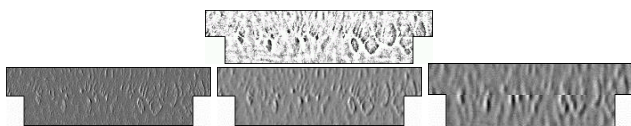


Figure 8. Iris images obtained by quadratic spline wavelet transform ( $j=1, 2, 3$ , from left to right): (a) original image, (b)  $x$ -direction WT,  $W_{2^j}^1 f(u, v)$ , (c)  $y$ -direction WT,  $W_{2^j}^2 f(u, v)$ , (d) WT modulus,  $M_{2^j} f(u, v)$ , and (e) WT gradient direction,  $A_{2^j} f(u, v)$ .

### 4.3 The GDC Method: Gradient Direction Coding with Gray code

The first method, called the GDC method, we used here is gray coding that is a 2-D method and designed to encode the gradient direction of each small 2-D iris image block in WT domain. The scale of the wavelet representation we select in this method is  $j=4$ . The flowchart of feature extraction and encoding of the first method is depicted in Figure 9.

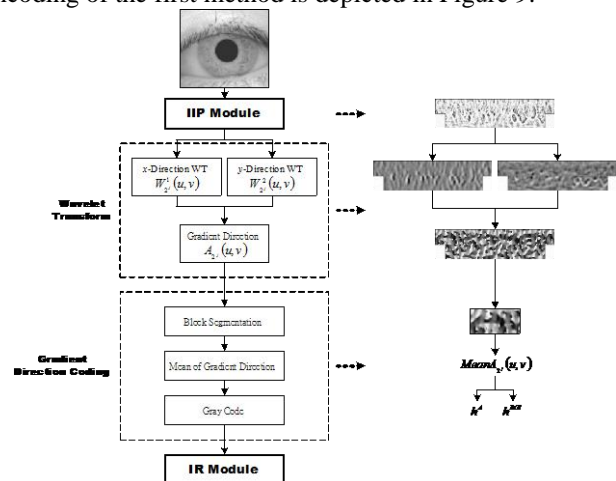


Figure 9. The flowchart of the feature extraction and encoding in the GDC method.

After demarcating the iris zone which contains two rectangles with the size  $256 \times 32$  pixels and two rectangles with the size  $212 \times 32$  pixels, we subdivide the four 2-D rectangular iris images in the WT gradient direction domain equally into 472 ( $8 \times 4$ ) small blocks. The mean of  $A_{2^j} f(u, v)$  of all pixels within each iris block is extracted as the edge feature of the block. Accordingly, 472 features for each input iris image are obtained. In order to reduce the code length of iris features and avoid affected by noises, we encode these features by using the Gray code concept, as shown in Figure 10. In the proposed gray code, the region of  $[0, 2\pi]$  is equally divided into eight intervals that each covers  $45^\circ$  and each interval is encoded by a 4-bit code. The codes corresponding to the adjacent intervals differ from only one bit, thus the Hamming distance between them is

minimum. On the other hand, the codes corresponding to the interval which differ 180° are different by all of the four bits, thus the Hamming distance between them is maximum. Which code is used to represent the block to be processed depends on which interval the mean gradient direction computed from each block belongs to. Furthermore, we add an equal number of masking bits referred to as ROI (region of interest) processing [29] to signify whether any iris region is obscured by eyelids and contains any eyelash occlusions. Hence, five bits are required to encode each block. In summary, a code vector of 295 bytes (including 59 bytes of ROI side information) totally is generated to represent an iris image by using the GDC method. We can use these iris code vectors for following pattern recognition.

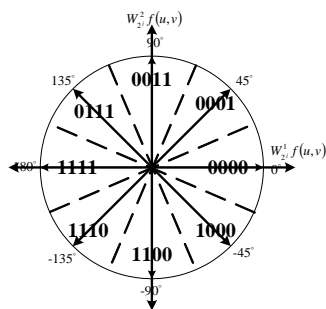


Figure 10. Encoding the features with Gray code.

#### 4.4 DMC Method: Delta Modulation Coding

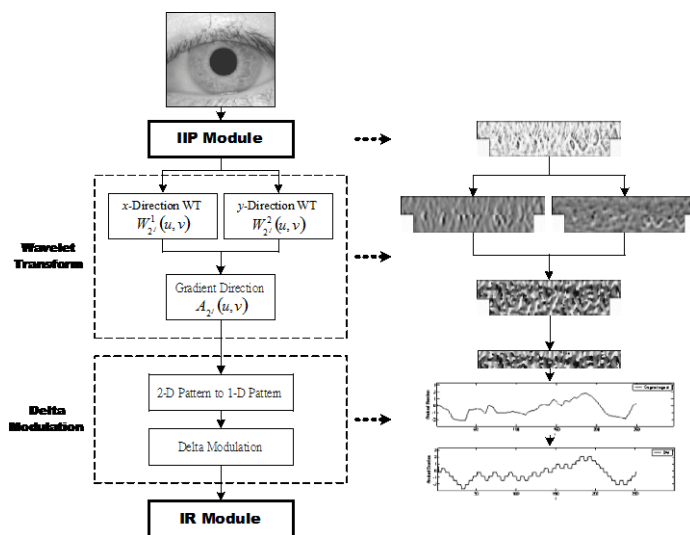


Figure 11. The flowchart of the feature extraction and encoding in the DMC method.

The second method is called the DMC method in which the delta modulation concept is used to efficiently encode the feature information. This is a 1-D method in which the 2-D feature information is converted into 1-D feature signals before encoding. The encoding method used here is delta modulation.

Delta modulation [28][29] is a DPCM (differential pulse-code modulation) scheme in which the difference signal is encoded into just a 1-bit quantizer. The single bit, providing for just two possibilities  $\pm\Delta$ , is used to increase or decrease the estimated signals. Here, we adopt two different types of delta modulation, linear delta modulation (DM) [28][29] and constant factor adaptive delta modulation (CFDM) [30], applied in the feature extraction module.

In this method, similar to the GDC method, we also use the information of gradient direction in the wavelet transform domain at a specific scale for recognition. The scale of the wavelet representation we select in this method is  $j=3$ . The flowchart of the DMC method is depicted in Figure 11. We first convert the 2-D iris blocks into 1-D signal with ring-projection [26] by computing the mean of gradient direction of each  $8 \times 1$  pixels block as a sampled point of the 1-D signal for reducing the dimensionality of two-dimensional image, as shown FIGURE 12. In order to acquire shorter code length; and further, the perpendicular texture of iris has more information entropy, we only select the two inner regions each with the size  $256 \times 16$ , which are closer to pupil, as the iris features because the two outer regions are easily polluted by the lower eyelid and eyelashes. Because of the conversion of 8 vertically consecutive pixels to a sampled point, we will obtain four 1-D discrete signals each with the length of 256 points. Totally, there are 1,024 feature points.

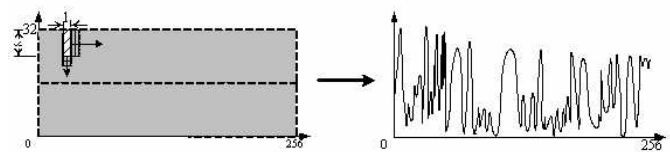


Figure 12. Conversion of 2-D feature information into 1-D feature signal.

After generating four 1-D patterns, we encode each of the patterns by the DM and CFDM methods. If encoding the features with the DM method, we initially select a step size  $\Delta=24$  and use sampling rate 1 Hz. With the CFDM method, the step size is set as  $\Delta=16$  and the same sampling rate as in the DM method is used. Furthermore, the adaptation logic used in the CFDM method is  $\{M_1=0.7, M_2=0.9, M_3=1.1, M_4=1.4\}$ . As a result, a code vector of 132 bytes is required to represent an iris image with the DM and CFDM coding methods.

#### 4.5 Recognition Module

In this module, the feature code vector extracted from the claimant iris image is compared against those of the enrolled feature code vectors in an iris database we created. Here for simplicity, we adopt the mean vector as the prototype of each

pattern class in the enrollment phase and utilize the minimum distance classifier to check the approach in the recognition phase [31]. When the feature code vector in the GDC method is compared, we calculate the normalized Hamming distance HD between two feature code vectors  $h_1$  and  $h_2$ , which is defined as

$$HD(h_1, h_2) = \min_{rad} \frac{\sum_k \sum_l (h_1^A(k-rad, l) \oplus h_2^A(k, l)) \times h_1^{ROI}(k-rad, l) \times h_2^{ROI}(k, l)}{\sum_k \sum_l h_1^{ROI}(k-rad, l) \times h_2^{ROI}(k, l)}$$

$$HD \in [0,1]$$

where the subscripts  $k, l$  denote indexing bit position,  $\oplus$  denotes the exclusive-OR operator, and  $rad$  denotes correcting the rotation effect of the input iris image. On the other hand, we adopt another metric for the DM and CFDM methods to calculate the normalized Euclidean distance  $D$  of feature vectors  $g_1$  and  $g_2$ , which is defined as

$$D(g_1, g_2) = \frac{1}{255 \cdot N} \min_{rad} \left( \sum_{m=1}^N (g_1(m+rad) - g_2(m))^2 \right)^{\frac{1}{2}}, D \in [0,1]$$

where  $m$  denotes the position of restructured signal and  $rad$  correcting the rotation effect of the input iris image. Both two minimum distance classifiers are normalized to  $[0, 1]$ .

### 5. EXPERIMENTAL RESULTS

To evaluate the performance of the proposed human iris recognition system, we implemented and tested the proposed schemes in this paper on the CASIA iris image database (Version 1.0) [23], built by Institute of Automation (IA), Chinese Academy of Sciences (CAS). It is composed of 756 iris images captured from 108 different eyes (hence 108 classes). Each original iris image has the resolution of 320×280 in gray level. For each eye, seven images are captured in two sessions, in which three samples are collected in the first session and four in the second session. It was suggested [23] that the recognition system compare two samples from the same eye taken in different sessions. For example, the iris images captured in the first session are employed as enrollment data set and those in the second session are used for testing.

In a verification system, the performance can be measured in terms of three different factors:

- (1) False Acceptance Rate (FAR): the probability of identifying an impostor as an enrolled user. The lower the FAR, the better the system;
- (2) False Rejection Rate (FRR): the probability of rejecting an enrolled user, as if he is an impostor. The lower the FRR, the better the system;
- (3) Equal Error Rate (EER): the value where the FAR and FRR rates are equal. The goal is to design a recognition system having an EER as lower as possible.

### 5.1 Results of Image Pre-processing

We check the accuracy of the boundaries (including pupil, iris, and lower eyelid) subjectively and the proposed system obtains the success rate of 82.54% (624 images) from 756 images in the experiments for the pre-processing module. Table 1 shows the summary of the causes of failure of image pre-processing. It is worth noting that the two main causes of failure come from occlusion by eyelids and non-uniform illumination.

Among those 624 images obtained successfully from the image pre-processing module, we select 587 images (90 classes) out of them for testing (enrollment and recognition). A half of 90 classes are regarded as legal users and the rest as impostors (illegal users). We train the system by selecting 3 images as the training image set for each person from the authorized users in the enrollment phase. Hence, there are 317 images for testing (160 images from the authorized users and 157 images from the impostors). By the following experiments, we can obtain the recognition performances for the proposed iris recognition system.

Table 1. Analysis of causes of failure for the image pre-processing module.

Causes of Failure		# of Data	Ratio (%)
(1)	Occlusion by eyelids or eyelashes	51	38.64%
(2)	Inappropriate eye positioning	2	1.52%
(3)	Pupil or iris is not a circular form	2	1.52%
(4)	Non-uniform illumination	71	53.79%
(5)	Affected by iris texture	3	2.27%
(6)	etc.	3	2.27%
<b>Total</b>		<b>132</b>	<b>100%</b>

### 5.2 Results of the GDC Method

In this experiment, we test the recognition performance for the GDC method. To obtain a threshold separating FRR and FAR, we perform two tests: one is for false rejection test (160 images) and the other is for false acceptance rate test (157 images). For the case of FRR, we can obtain the distribution of non-matching distance between the unknown classes and the registered classes. For the case of FAR, we also obtain the distribution of non-matching between the unknown classes for impostors and the registered classes. Figure 13 shows the distributions of the above two experiments. In this figure, the x-axis and y-axis indicate the number of data and the degree of distance, respectively.

Figure 14 shows the plot of the variation of FRR and FAR according to the distribution of non-matching distance by selecting a proper distance threshold. When we set the threshold to be 0.3775, the system obtains the recognition performance of about EER=4.73%. And when the FAR is set to be 0%, the system can obtain FRR=6.88% at a threshold of 0.36. In particular, if we use a code vector of 585 bytes instead of 295 bytes, the recognition performance of the proposed system can be lower to 0.95% only. The experimental results show that the proposed system performs well.

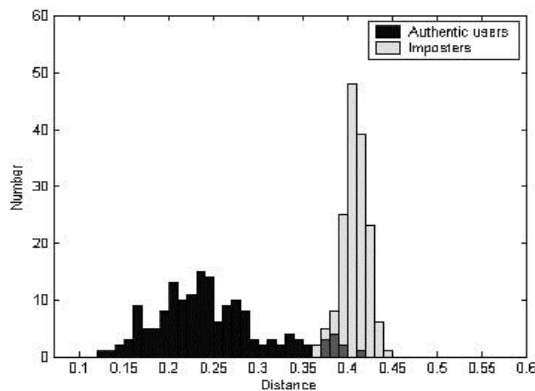


Figure 13. The distribution of non-matching distance of feature vectors in the GDC method.

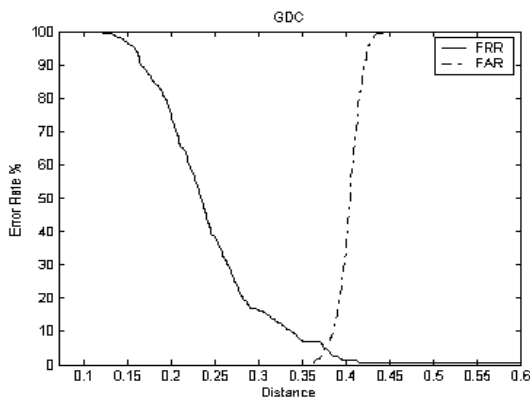


Figure 14. Variation of FRR and FAR vs. non-matching distance in the GDC method.

### 5.3 Results of the DMC Method

In this experiment, we test the performance for the DM and CFDM methods separately as the previous method. In the DM method, we obtain the distribution of non-matching distance for FRR experiment and FAR experiment, as shown in Figure 15. Figure 16 shows the plot of the variation of FRR and FAR in the DM method by selecting a proper distance threshold. By selecting the threshold of 0.1785, the system obtains the system performance of EER=4.38%. Similarly, if the FAR is set to be 0%, the system can obtain FRR=9.38% at a threshold of 0.173.

Next, we perform the same experiments for the CFDM method. The system obtains two distributions of FRR and FAR, respectively, as shown in Figure 17. Figure 18 shows the plot of the variation of FRR and FAR in the CFDM method. The system performance is about EER=3.79% by selecting the threshold of 0.1645. Similarly, if FAR is set to be 0%, the system can obtain FRR=8.13% at a threshold of 0.159. The experimental results show that the CFDM method can perform better slightly than the DM method. The superiority of the CFDM method should come from the fact that it is an adaptive approach.

Finally, we make a summary of the experimental results in Table 2. It can be seen from the results that both the DM and CFDM methods have a superior performance to the GDC method by comparing the EER performance. On the other hand, the DM method can perform superiorly in the case of FAR=0%. Consequently, the GDC method provides a securer system than the DM methods.

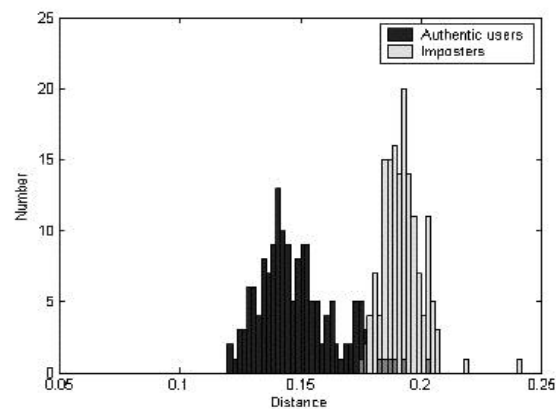


Figure 15. The distribution of non-matching distance of feature vectors in the DMC method.

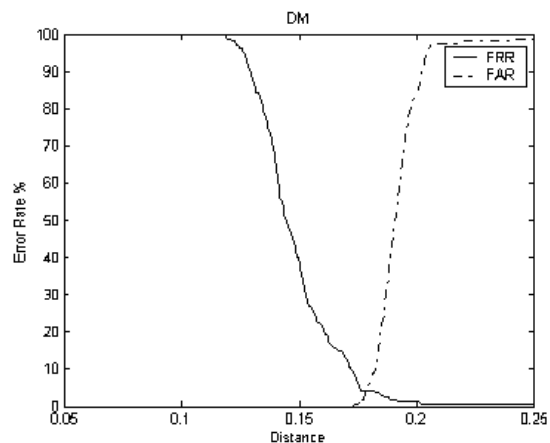


Figure 16. Variation of FRR and FAR vs. non-matching distance in the DMC method.

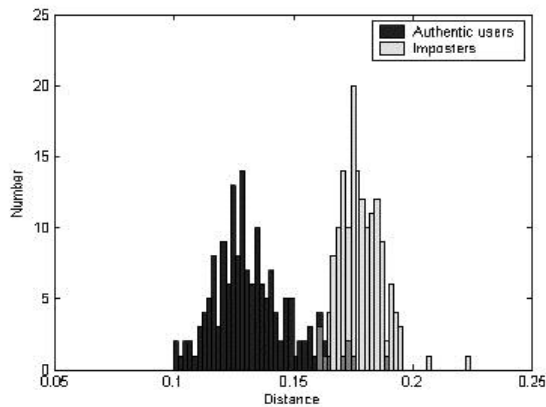


Figure 17. The distribution of non-matching distance of feature vectors in the CFDM method.

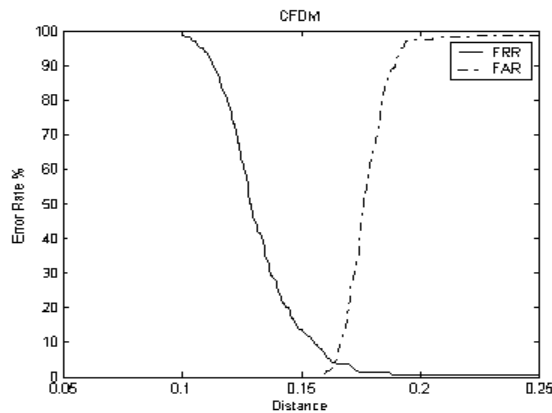


Figure 18. Variation of FRR and FAR vs. non-matching distance in the CFDM method.

Table 2. Identification accuracy of the GDC, DM, and CFDM methods.

Mode	IFE Module	Size of Features	RA (%)	AA (%)	AF (%)	RF (%)
ERR	GDC	585 bytes	0.95 %	99.05 %	0.95 %	99.05%
	GDC	295 bytes	4.73 %	95.27 %	4.73 %	95.27%
	GDC	147 bytes	5.94 %	94.06 %	5.94 %	94.06%
	DM	132 bytes	4.38 %	95.62 %	4.38 %	95.62%

	CFDM	132 bytes	3.79 %	96.21 %	3.79 %	96.21%
FAR = 0%	GDC	295 bytes	6.88 %	93.12 %	0.00 %	100.00 %
	GDC	147 bytes	7.50 %	92.50 %	0.00 %	100.00 %
	DM	132 bytes	9.38 %	90.62 %	0.00 %	100.00 %
	CFDM	132 bytes	8.13 %	91.87 %	0.00 %	100.00 %

6. CONCLUSION

In this paper, a personal identification technique with human iris recognition based on wavelet transform has been proposed. The image pre-processing module can determine the quality of input images correctly. And we use three different methods, including GDC, DM, and CFDM, in the feature extraction module. All the methods can obtain a good recognition rate. If the system set FAR to be 0%, the recognition rates can approach more than 90%. If we increase the size of feature code, for example, to 585 bytes, the performance gets better, even up to 99%. From the experimental result, it is shown that the proposed iris recognition technique is suitable for the environment in high security level.

REFERENCES

- [1] A. K. Jain, R. Bolle and S. Pankanti, *Biometrics: Personal Identification in Network Society*. Kluwer Academic Publishers, 1999.
- [2] B. Miller, "Vital signs of identity," *IEEE Spectrum*, pp. 22-30, Feb. 1994.
- [3] A. K. Jain, L. Hong, S. Pankanti and R. Bolle, "An identity-authentication system using fingerprints," *Proceedings of the IEEE*, vol. 85, No. 9, pp. 1365-1376, Sept. 1997.
- [4] D. Zhang and W. Shu, "Two novel characteristics in palmprint verification: datum point invariance and line feature matching," *Pattern Recognition*, vol. 32, pp. 691-702, 1999.
- [5] R. Chellappa, C. L. Wilson and S. Sirohey, "Human and machine recognition of faces: a survey," *Proceedings of the IEEE*, vol. 83, No. 5, pp. 705-740, May 1995.
- [6] F. Leclerc and R. Plamondon, "Automatic signature verification: the state of the art --- 1989-1993," *International Journal of Pattern Recognition and Artificial Intelligence*, vol. 8, No. 3, pp. 643-660, Jun. 1994.
- [7] H. Gish and M. Schmidt, "Text-independent speaker identification," *IEEE Signal Processing Magazine*, vol. 11, No. 4, pp. 18-32, Apr. 1994.
- [8] K. Inman and N. Rudin, *An Introduction to Forensic DNA Analysis*, CRC Press, Boca Raton, Florida, 1997.
- [9] R. B. Hill, "Apparatus and method for identifying individuals through their retinal vasculature patterns," *US patent No. 4 109 237*, 1978.
- [10] L. Flom and A. Safir, "Iris recognition system," *U.S. Patent 4 641 349*, 1987.

- [11] R. G. Johnson, "Can iris patterns be used to identify people?" Chemical and Laser Sciences Division, LA-12331-PR, Los Alamos National Laboratory, Los Alamos, CA, 1991.
- [12] J. G. Daugman, "High confidence visual recognition of persons by a test of statistical independence," *IEEE Trans. on Pattern Analysis and Machine Intelligence*, vol. 15, No. 11, pp. 1148-1161, Nov. 1993.
- [13] R. P. Wildes, *et al.*, "A machine-vision system for iris recognition," *Machine Vision and Applications*, Springer-Verlag, 1996.
- [14] R. P. Wildes, "Iris recognition: an emerging biometric technology," *Proceedings of the IEEE*, vol. 85, No. 9, pp. 1348-1363, Sep. 1997.
- [15] M. Negin, *et al.*, "An iris biometric system for public and personal use," *IEEE Computer Magazine*, pp. 70-75, Feb. 2000.
- [16] C.-T. Chou, S.-W. Shih, W.-S. Chen V. W. Cheng and D.-Y. Chen, "Non-orthogonal view iris recognition system," *IEEE Trans. on Circuits and Systems for Video Technology*, vol. 20, No. 3, pp. 417-430, Mar. 2010.
- [17] W. W. Boles and B. Boashash, "A human identification technique using images of the iris and wavelet transform," *IEEE Trans. on Signal Processing*, vol. 46, No. 4, pp. 1185-1188, Apr. 1998.
- [18] Y. Zhu, T. Tan and Y. Wang, "Biometric personal identification based on iris patterns," *Proc. of International Conference on Pattern Recognition*, vol. II, pp. 801-804, 2000.
- [19] L. Ma, Y. Wang and T. Tan, "Iris recognition using circular symmetric filters," *Proc. of International Conference on Pattern Recognition*, vol. II, pp. 414-417, 2002.
- [20] L. Ma, T. Tan, Y. Wang and D. Zhang, "Personal identification based on iris texture analysis," *IEEE Trans. on Pattern Analysis and Machine Intelligence*, vol. 25, No. 12, pp. 1519-1533, Dec. 2003.
- [21] S. Lim, K. Lee, O. Byeon and T. Kim, "Efficient iris recognition through improvement of feature vector and classifier," *ETRI Journal*, vol. 23, June 2001.
- [22] M. Nabti and A. Bouridane, "An effective and fast iris recognition system based on a combined multiscale feature extraction technique," *Pattern Recognition*, vol. 41, No. 3, pp. 868-879, Mar. 2008.
- [23] Institute of Automation, Chinese Academy of Sciences, *CASIA Iris Image Database*, <http://www.sinobiometrics.com/>.
- [24] S. Mallat, *A Wavelet Tour of Signal Processing*, 2<sup>nd</sup> Edition, Academic Press, San Diego, 2001.
- [25] S. Mallat and S. Zhong, "Characterization of signals from multiscale edge," *IEEE Trans. on Pattern Analysis and Machine Intelligence*, vol. 14, No. 7, pp. 710-732, July 1992.
- [26] Y. Y. Tang, *et al.*, *Wavelet Theory and Its Application to Pattern Recognition*, World Scientific, Singapore, 2000.
- [27] J. Canny, "A computational approach to edge detection," *IEEE Trans. on Pattern Analysis and Machine Intelligence*, vol. 8, No. 6, pp. 679-698, 1986.
- [28] S. Haykin, *Communication Systems*, 4th Edition, John Wiley & Sons, 2000.
- [29] H. Schindler, "Linear, nonlinear, and adaptive delta modulation," *IEEE Trans. on Communications*, vol. 22, pp. 1807-1823, Nov. 1974.
- [30] K. Sayood, *Introduction to Data Compression*, 2nd Edition, Morgan Kaufmann, 2000.
- [31] R. C. Gonzalez and R. E. Woods, *Digital Image Processing*, 2nd Edition, Prentice-Hall, New Jersey, 2002.



Wen-Shiung Chen received M.S. degree from National Taiwan University, Taipei City, Taiwan, in 1985, and the Ph.D. degree from University of Southern California, Los Angeles, in 1994, both in electrical engineering. He was with Department of Electrical Engineering, Feng Chia University, Taichung, Taiwan from 1994 to 2000. In 2000, he joined Department of Electrical Engineering, National Chi Nan University, Puli, Nantou, Taiwan, where he is currently a Professor. His research interests include image processing, pattern recognition, computer vision, biometrics, mobile computing, and networking.



Kun-Huei Chih received M.S. degree in electrical engineering in 2004 from National Chi Nan University, Nantou, Taiwan, R.O.C.. His research interests include image processing and biometrics.